

# Bimodality: a possible experimental signature of the liquid-gas phase transition of nuclear matter

M. Pichon<sup>a</sup>, B. Tamain<sup>a</sup>, R. Bougault<sup>a</sup>, F. Gulminelli<sup>a</sup>,  
 O. Lopez<sup>a</sup>, E. Bonnet<sup>c</sup>, B. Borderie<sup>c</sup>, A. Chbihi<sup>b</sup>, R. Dayras<sup>d</sup>,  
 J.D. Frankland<sup>b</sup>, E. Galichet<sup>i</sup>, D. Guinet<sup>e</sup>, P. Lautesse<sup>e</sup>,  
 N. Le Neindre<sup>c</sup>, M. Pârlog<sup>f</sup>, M.F. Rivet<sup>c</sup>, R. Roy<sup>h</sup>, E. Rosato<sup>g</sup>,  
 E. Vient<sup>a</sup>, M. Vigilante<sup>g</sup>, C. Volant<sup>d</sup>, J.P. Wieleczko<sup>b</sup>,  
 B. Zwieglinski<sup>j</sup>

INDRA and ALADIN collaborations

<sup>a</sup>*LPC, IN2P3/CNRS, ENSICAen and University, F-14050 Caen cedex, France*

<sup>b</sup>*GANIL, DSM-CEA/IN2P3-CNRS, BP 5027, F-14076 Caen cedex 5, France*

<sup>c</sup>*IPN, IN2P3/CNRS, BP 1, F-91406 Orsay cedex, France*

<sup>d</sup>*DAPNIA/SPhN, CEA/SAclay, F-91191 Gif-sur-Yvette cedex, France*

<sup>e</sup>*IPN, IN2P3/CNRS and University, F-69622 Villeurbanne cedex, France*

<sup>f</sup>*Nat. Inst. for Phys. and Nucl. Eng., RO-76900 Bucharest-Magurele, Romania*

<sup>g</sup>*Dip. di Sci. Fis. Sez. INFN, Univ. di Napoli, "Frederico II", I-80126 Napoli, Italy*

<sup>h</sup>*Laboratoire de Physique Nuclaire, Universit Laval, Qubec, Canada*

<sup>i</sup>*CNAM, Laboratoire des Sciences Nuclaires, F-75003 Paris, France*

<sup>j</sup>*Soltan Institute for Nuclear Studies, 00-681 Warsaw, Poland*

---

## Abstract

We have observed a bimodal behaviour of the distribution of the asymmetry between the charges of the two heaviest products resulting from the decay of the quasi-projectile released in binary Xe+Sn and Au+Au collisions from 60 to 100 MeV/u. Event sorting has been achieved through the transverse energy of light charged particles emitted on the quasi-target side, thus avoiding artificial correlations between the bimodality signal and the sorting variable. Bimodality is observed for intermediate impact parameters for which the quasi-projectile is identified. A simulation shows that the deexcitation step rather than the geometry of the collision appears responsible for the bimodal behaviour. The influence of mid-rapidity emission has been verified. The two bumps of the bimodal distribution correspond

to different excitation energies and similar temperatures. It is also shown that it is possible to correlate the bimodality signal with a change in the distribution of the heaviest fragment charge and a peak in potential energy fluctuations. All together, this set of data is coherent with what would be expected in a finite system if the corresponding system in the thermodynamic limit exhibits a first order phase transition.

---

## 1 Introduction

Many experimental features suggestive of the liquid-gas phase transition of nuclear matter have been observed in the Fermi energy regime of nucleus-nucleus collisions. Among these features are: abnormal partial energy fluctuations[1,2], charge correlations[3], a double peaked distribution of an order parameter ("bimodality")[4,5], fluctuation properties of the heaviest fragment size[6,7], Fisher scaling[8], vaporisation[9], flattening of the caloric curve[10,11]. In the present paper, we concentrate on the bimodality signal.

The discontinuity of the order parameter at a first order phase transition is expected to be replaced in a finite system by a bimodal distribution of the order parameter close to the transition point[12]. If the order parameter is one dimensional[15] and if the transition has a finite latent heat, the bimodality should be observed in the canonical ensemble, the transition temperature being defined as that at which the two peaks have the same height [13]. In the fragmentation transition case, the size of the heaviest cluster produced in each event is an order parameter in many different models[14] including the lattice-gas model of the liquid-gas phase transition[15]. In this picture, when the size of the heaviest fragment is large, the system is mostly on the liquid-like side, whereas if it is small one is mostly dealing with a gas-like behaviour.

An example is given in figure 1 obtained in the lattice-gas approach (see for instance ref[16][13]). For temperatures outside of a small range around the transition temperature, the size of the largest fragment exhibits single-humped distributions whereas two peaks of the same height are obtained at the transition temperature value. This result which is obtained for an equilibrated system in the canonical isobar ensemble remains approximately valid even if part of the available energy is not thermalized. This is shown in figure 2 in which an aligned momentum has been randomly added for each particle, which simulates the dynamical effects corresponding to the memory of the aligned beam momentum in the entrance channel. Several percentages of aligned momenta have been considered ranging from zero percent (purely thermal situation) to 100 percent (same amount of aligned and thermalized momentum). The bimodality signal is robust in the sense that it is observed even if a sizeable amount of the total available momentum is still aligned along

the beam direction, with only a slight change of the deduced transition temperature. Only if the aligned momentum is as important as the thermal one (lower right in the figure) the distribution is weakly bimodal and mimics a flat distribution expected for a continuous transition[12,14].

Guided by these considerations, preliminary evidences of bimodal behaviours in some static observables have been obtained in previous data concerning the systems Ni+Au[18], Ni+Ni[19], and Xe+Sn[20]. In none of these cases, a clear bimodality was observed in the distribution of the heaviest fragment charge. A possible reason is that references [18,19,20] concern central collisions. In such cases, the event selection is closer to a microcanonical sorting, with a selection of a narrow range of excitation energy: if the transition is characterized by a finite latent heat, the two peaks that can be interpreted as precursors of the two coexisting phases[16] should be associated to two different energies. The signal which would naturally appear if the system was in contact with a heat bath is expected to be quenched if the experimental sorting constrains too strongly the deposited excitation energy.

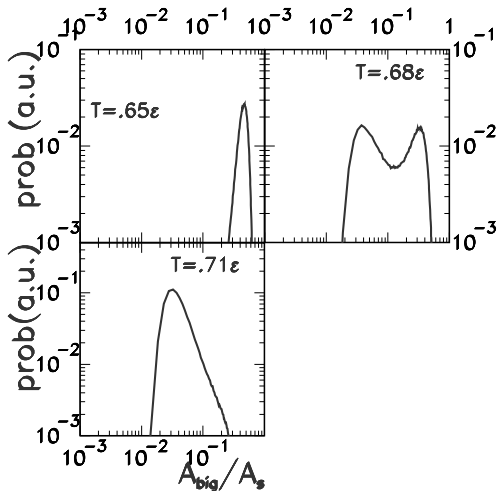


Fig. 1. Size distribution of the largest product obtained with the lattice-gas model for an equilibrated system of 216 particles in the canonical isobar ensemble at subcritical pressure[13].  $\epsilon$  represents the lattice coupling. The three plots correspond to temperatures respectively below, at and above the transition one.

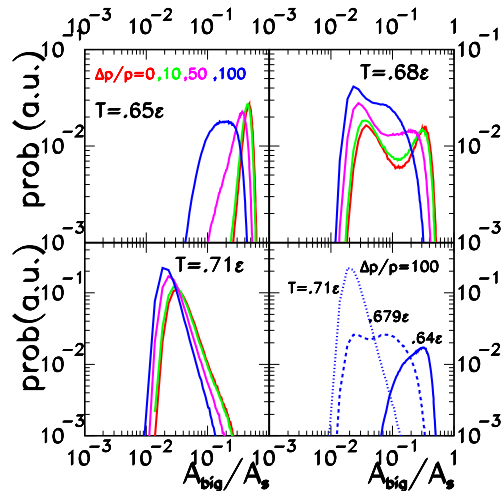


Fig. 2. Similar to figure 1 but an aligned momentum component has been added for each particle. The added aligned momentum is 0, 10, 50 or 100 percent of the thermalized one. The last insert corresponds to the 100 percent case at three different temperatures. Such calculations which include an out-of-equilibrium component are presented in reference[13].

In order to mimic a canonical sorting in the data selection, one can select semi-peripheral collisions which are mostly binary. In these collisions, it is possible to isolate a quasi-projectile (QP) and a quasi-target (QT). The fluctuations in the sharing of the dissipated energy between these two partners may be

sufficient to explore the two phases. In the present work, we focus on such peripheral and semi-peripheral collisions.

## 2 The experiment

The data have been obtained by the Indra-Aladin collaboration (Indra at GSI). The Indra set up is described in references[21,22], while details of the measurements performed at the GSI laboratory and of the analysis and calibration procedures may be found in [23,24,25,26]. The studied systems are Xe+Sn and Au+Au from 60 to 100 MeV/u. The events were registered if at least four modules fired. In this section the question of the event sorting is first addressed. Then we will check to which extent it is possible to isolate properly the QP from the QT and any mid-rapidity emission.

### 2.1 Event sorting

In order to separate the QP and QT contributions, the momentum tensor calculated from  $Z \geq 3$  products has been diagonalized event by event. The main axis of the tensor is in most cases close to the beam axis. The particles and fragments attributed to the QT (resp. QP) are those which are backward (resp. forward) emitted along the main tensor axis. Event sorting has been achieved from the transverse energy  $E_{trans}$  of light charged particles (LCP) on the QT side calculated in this frame. A selected  $E_{trans}$  value corresponds to a selected violence of the collision.

The  $E_{trans}$  sorting has the advantage of minimizing autocorrelations between the sorting variable and observables, since the sorting particles are only loosely correlated to the particles and fragments considered to get the QP properties. From the experimental point of view, the detection efficiency is good for LCP in the whole space since the LCP detection thresholds are small. Hence, the LCP transverse energy on the QT side was well measured. On the other hand, the detection efficiency on the QP side (velocities exceeding the c.m. velocity) is good for both the LCP and the fragments since all the laboratory velocities are far above the detection thresholds for any product. In order to ensure an almost complete QP reconstruction, any event for which the forward detected charge was below 80 percent of the projectile charge has been rejected. This selection rejected mainly peripheral events for which the QP residue was emitted in the forward detector opening.

The  $E_{trans}$  distributions, normalized to the size of the system and to the laboratory bombarding energy in MeV/u, for different systems are shown in

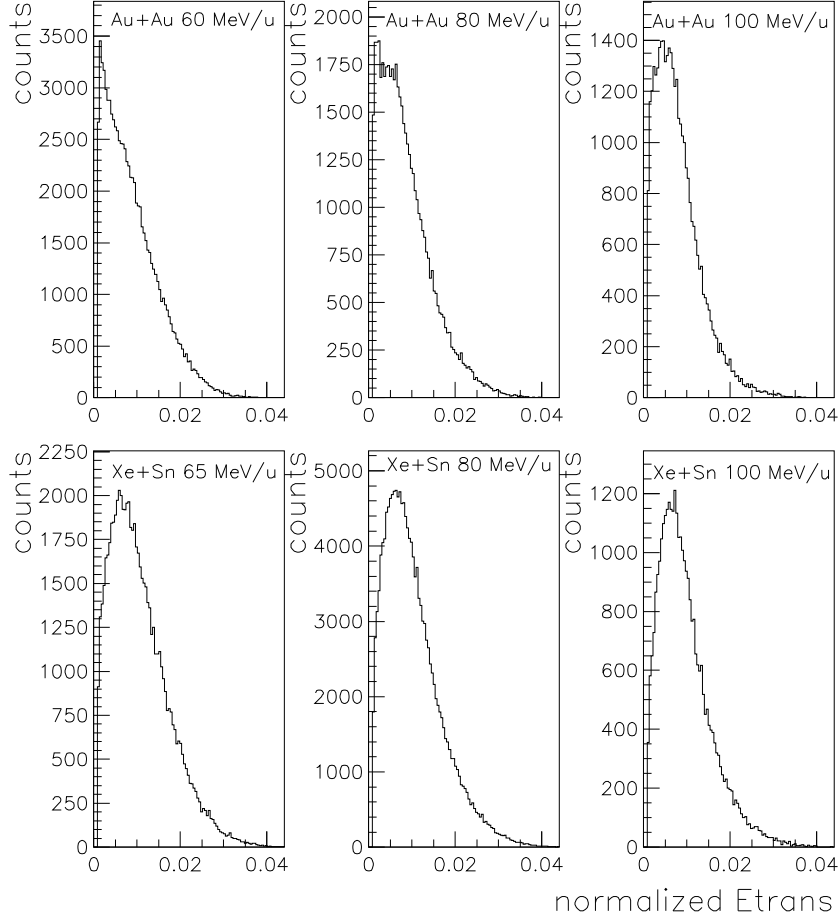


Fig. 3. *Etrans* distributions for the two studied systems at the three indicated energies. For the abscissa *Etrans* has been divided by the total mass number of the system (projectile + target), and by the incident energy in MeV/u.

figure 3. They are similar and they extend on the same abscissa range whatever the system and the incident energy. The differences between the systems are mainly due to the loss of efficiency for very peripheral collisions when the quasi-projectile residue escapes in the detector forward hole (these events are rejected because of the completeness detection criterion). This efficiency loss is stronger for the lighter system because QP fission has a negligible probability in the Xe mass range: the QP loss in the forward hole is indeed reduced when fission occurs because the fission fragment emission angles are generally pushed away from very forward directions.

The similarity of the various normalized-*Etrans* distributions indicates that the energy damping (or the stopping power) does not depend strongly on the mass number nor on the available energy in this bombarding energy region. It is in agreement with the conclusions of reference[27]. The largest values reached by the normalized *Etrans* are about 0.04. They can be compared with the limiting value of  $1/12 \sim 0.08$  which would correspond (for such symmetrical systems) to a complete fusion followed by vaporization (with

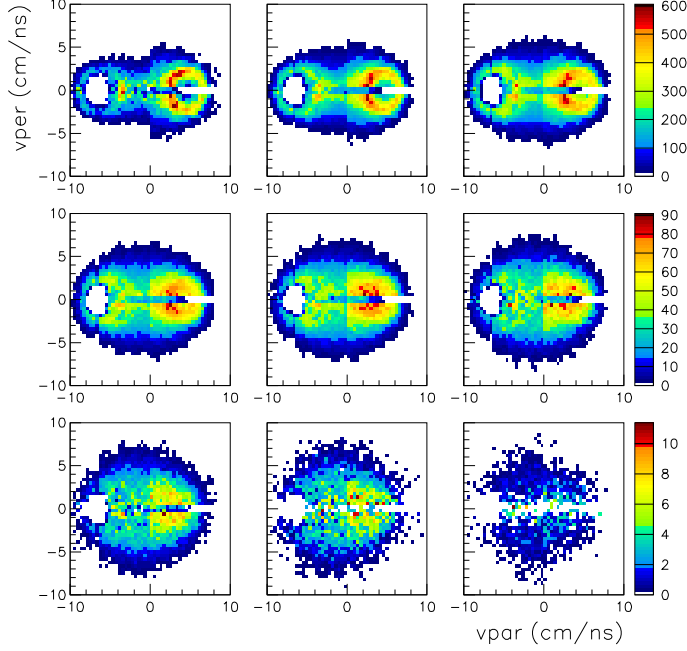


Fig. 4. Alpha particle centre-of-mass  $v_{par} - v_{per}$  plots for nine  $E_{trans}$  bins covering the whole  $E_{trans}$  distribution of figure 3. Xe+Sn system at 80 MeV/u. The width of each  $E_{trans}$  bin is 100 MeV i.e. 0.4 MeV/u if  $E_{trans}$  is normalized on the total system mass as in figures 11 and 12

only LCPs as decay products).

## 2.2 Kinematical separation between QP and QT decay products

This paper is devoted to the QP decay study. Hence, it must be verified to which extent the QP and QT decay products can really be separated. This question can be answered looking at figure 4 in which typical  $v_{par} - v_{perp}$  invariant cross section plots are shown for alpha particles emitted in 80 MeV/u Xe on Sn collisions.  $v_{par}$  and  $v_{per}$  are the parallel and perpendicular velocity components in the reaction centre of mass frame. Similar distributions are obtained for the other systems considered in this paper. The events have been sorted in nine  $E_{trans}$  bins. The distributions clearly exhibit two sources for peripheral and semi-peripheral collisions at least up to the fourth bin. For the highest  $E_{trans}$  values the distinction between a QP and a QT source becomes somewhat artificial.

A careful observation of figure 4 indicates that alpha particles are not isotropically emitted from the QP and QT. Instead more alphas are emitted at mid-rapidity in the neck region. This result is a general feature in intermediate energy nucleus-nucleus collisions[28,29,30] and one may worry about the influence of a mid-rapidity emission on the results discussed in this paper. This

will be discussed in section 5.

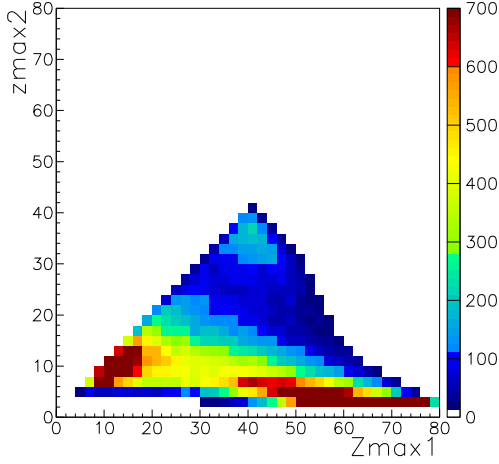


Fig. 5. Correlation between the second largest charge  $Zmax_2$  and the largest charge  $Zmax_1$  for the Au+Au system at 80 MeV/u.

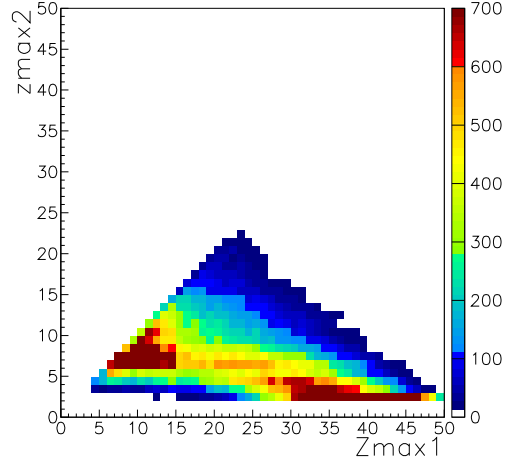


Fig. 6. Correlation between the second largest charge  $Zmax_2$  and the largest charge  $Zmax_1$  for the Xe+Sn system at 80 MeV/u.

### 3 QP observables

Following the discussion of the introduction, a natural choice of the order parameter is the size (charge) of the largest fragment  $Zmax_1$ . The asymmetry  $Z_{asym}$  between the two heaviest products  $Zmax_1$  and  $Zmax_2$  (see below equation 1 for its precise definition) will also be studied.

In figures 5 and 6, the correlations between  $Zmax_1$  and  $Zmax_2$  are shown for the Au+Au and Xe+Sn systems, respectively, at 80 MeV/u. All the retained (complete) events are included in the picture. For the Au+Au system, the binary fission of the quasi-gold nucleus can be recognized for  $Zmax_1$  and  $Zmax_2$  values around 40 charge units. This fission contribution is negligible for the Xe case. For both reactions one recognizes also two dominant classes of events. Residue like events correspond to a large  $Zmax_1$  and a small  $Zmax_2$ . Multifragmentation events correspond to small values for both  $Zmax_1$  and  $Zmax_2$ . An important feature is that there is not a continuous evolution from one class of events to the other. Instead, they are widely separated showing that they correspond to two clearly distinct mechanisms.

For Au QP, the presence of the fission channel perturbs the evolution of  $Z_{asym}$  since this variable exhibits similar values for multifragmentation and binary fission. In order to avoid this difficulty, we applied a specific treatment to the fission events observed for the Au case. In effect, they belong also to the normal compound nucleus decay event class and can be classified together

with the residue events. For this purpose, we defined  $Z_{max}$  as the sum of the two fission fragment charges when fission was recognized. Fission events have been selected from the charge product of the two fission fragments: charge product exceeding 900[1] (see also figure 5). For these events,  $Z_{max}$  is the sum of the two heaviest products and we defined  $Z_{sec}$  as the third heaviest product charge. For the other Au events and for any event in the Xe case (for which the fission contribution is negligible), one has  $Z_{max} = Z_{max_1}$  and  $Z_{sec} = Z_{max_2}$ . Then the asymmetry parameter is defined by:

$$Z_{asym} = \frac{Z_{max} - Z_{sec}}{Z_{max} + Z_{sec}} \quad (1)$$

In order to avoid spurious peaks due to integer number effects we have added a random number between -0.5 and +0.5 to  $Z_{max}$  and  $Z_{sec}$ . Thus  $Z_{asym}$  can exceed slightly the range [0-1].

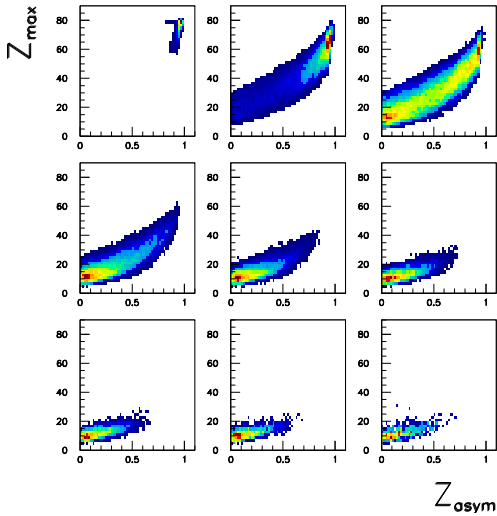


Fig. 7.  $Z_{max} - Z_{asym}$  plots for the nine  $E_{trans}$  bins. Au+Au system at 80 MeV/u.

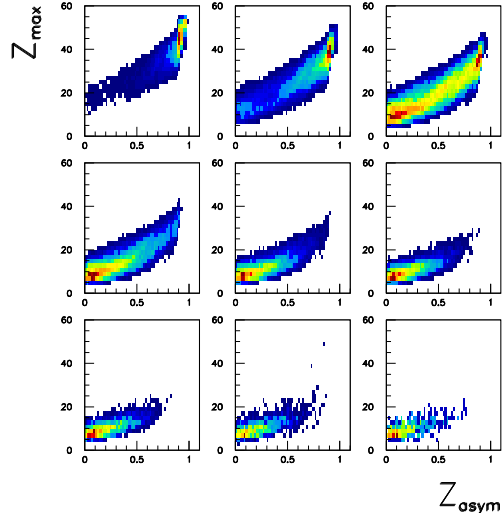


Fig. 8.  $Z_{max} - Z_{asym}$  plots for the nine  $E_{trans}$  bins. Xe+Sn system at 80 MeV/u.

#### 4 Bimodality observation

Let us consider now the evolution of the correlation between  $Z_{max}$  and  $Z_{asym}$  when the events are sorted according to the transverse energy  $E_{trans}$  defined in section 2.1. Figures 7 and 8 correspond to the systems Au+Au and Xe+Sn, respectively, at 80 MeV/u. They show the correlations between the asymmetry variable  $Z_{asym}$  and the heaviest product charge  $Z_{max}$  for the nine  $E_{trans}$  bins already used in figure 4. Two behaviours are clearly evidenced in the figures. In the first bins, the heaviest decay product is generally a residue (large  $Z_{max}$  and



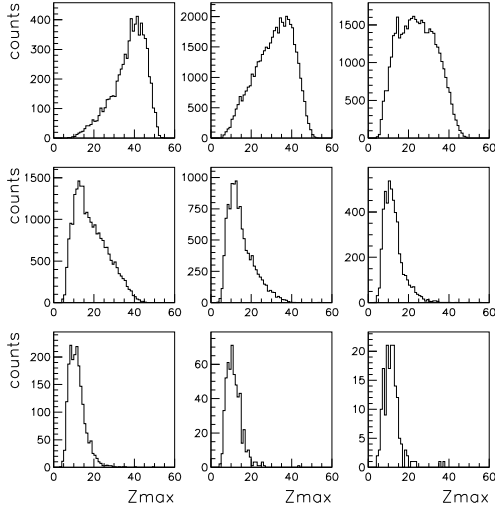


Fig. 9.  $Z_{max}$  distributions for the 9 *Etrans* bins. Xe+Sn system at 80 MeV/u.

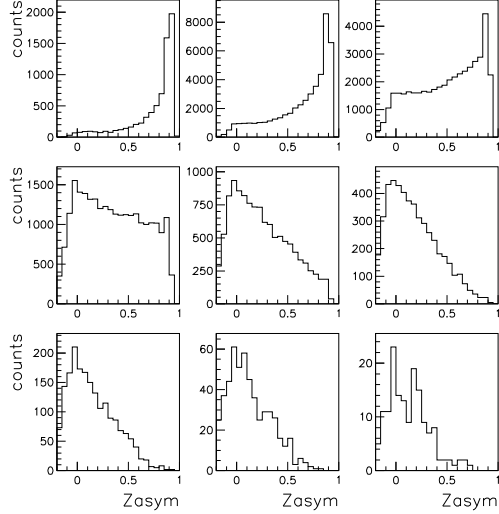


Fig. 10.  $Z_{asym}$  distributions for the 9 *Etrans* bins. Xe+Sn system at 80 MeV/u.

$Z_{asym}$  value close to unity). By contrast, the most violent (central) collisions correspond to small values of  $Z_{max}$  and  $Z_{asym}$  associated with multi-fragment emission (such observations are quite in agreement with the results of ref [31]). In between, in the third bin, both behaviours are observed: the distribution is bimodal. Similar results have been obtained by Ma et al[32] on a lighter system. Here we have such an observation on medium and large mass systems. With the definition of  $Z_{max}$  as the sum of the two fission fragment charges (see the previous section), the fission event behaviour is quite similar to the residue one. We have checked that, if one does not reconstruct the parent nucleus charge before fission, these events correspond to an additional bump in figure 7 widely separated from the residue and the fragmentation bumps. It does not modify the bimodality behaviour observed in the third bin.

Although the event probability distribution in the third bin exhibits a minimum in the representation of figures 7 and 8, this minimum (convex shape) is not apparent on the projections on the two axes, as shown in figures 9 and 10 for the Xe+Sn system at 80 MeV/u. Nevertheless, these figures indicate that the most probable values of the  $Z_{max}$  or  $Z_{asym}$  distributions change dramatically between the third and the fourth bins. This evolution is summarized in figures 11 and 12 for the two studied systems and the three bombarding energies. In these figures, the abscissa is the transverse energy sorting parameter *Etrans* divided by the system size (sum of the projectile and target masses).

The abrupt change of the order parameter together with the wide and almost structureless distribution at the transition point shown in figures 7-10 are rather suggestive of a continuous (second order) transition point. However, as we have discussed in section 1, such a behaviour is also consistent with a

first order transition polluted by strong out of equilibrium effects, or important deformations due to sorting constraints[15]: if the sorting variable is too strongly connected to the order parameter, its bimodal character is naturally suppressed.

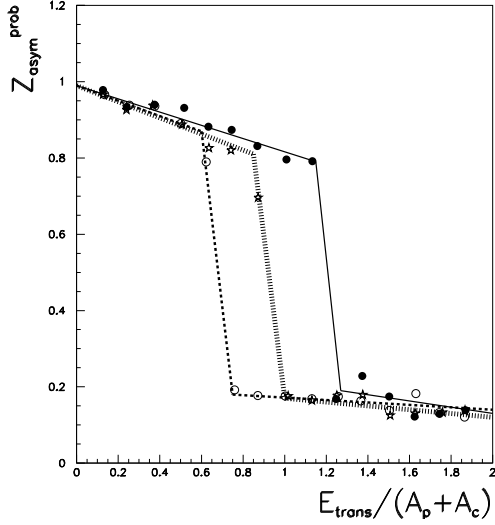


Fig. 11. System Au + Au at 60, 80, 100 MeV/u (respectively open points, stars and black points). Evolution with  $E_{trans}$  of the most probable value of the  $Z_{asym}$  distributions. In this figure,  $E_{trans}$  has been divided by the total mass number of the system (projectile + target). It has not been divided by the incident energy as in figure 3.

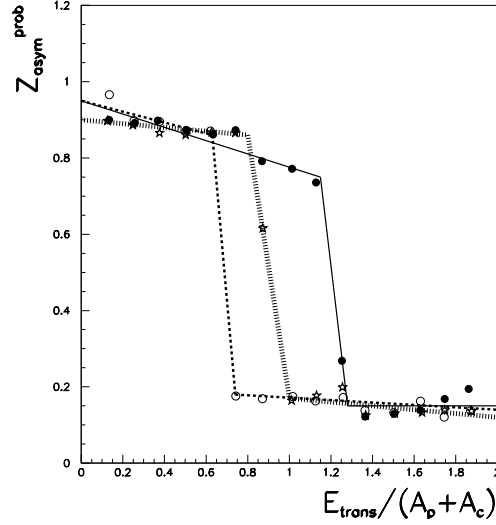


Fig. 12. Similar to figure 11 but for the systems Xe + Sn at 65, 80 and 100 MeV/u. The abscissa corresponding to the transitions are similar for Au + Au and Xe + Sn system. This scaling indicates that the transverse energy per nucleon is a key parameter.

## 5 Is bimodality due to dynamics?

In comparing figures 11 and 12, one may conclude that the transverse energy per nucleon at which the transition occurs does not depend on the system size. A similar kind of universality has also been pointed out in reference [33]. Such a result is expected if the transition reflects the energy density involved in the reaction. The transition energy for a definite system evolves when the bombarding energy increases: it is roughly proportional to the incident energy. This result is not expected if  $E_{trans}$  reflects the thermal energy stored in the quasi-projectile.

However,  $E_{trans}$  reflects both the dissipated energy and preequilibrium effects. When one increases the bombarding energy, the preequilibrium contribution increases thus inducing a larger value of  $E_{trans}$  to reach the same thermal energy. A similar behaviour has been evidenced from the calculations

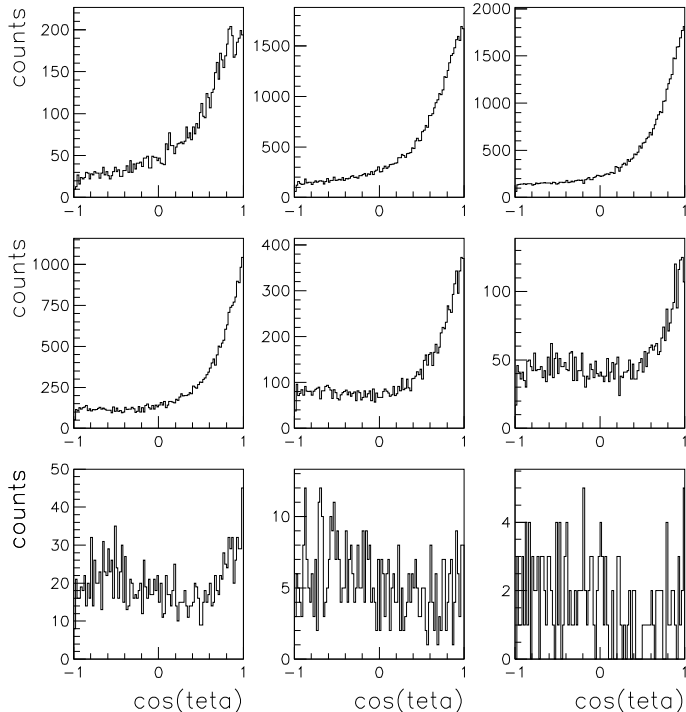


Fig. 13. Angular distributions of the heaviest QP fragment in the QP frame. The abscissa is the cosine of the angle between the QP direction in the centre of mass system and the  $Z_{max1}$  fragment direction in the QP frame. The events have been sorted according to the  $E_{trans}$  variable. Most of the heaviest fragments are forward emitted. Xe+Sn system at 80 MeV/u.

discussed in figure 2. To test such an interpretation, we have to introduce an additional selection of the events in order to decrease the influence of preequilibrium effects. Section 5.3 is devoted to the corresponding data analysis.

One may also consider that the transition (where bimodality is observed) corresponds to an intermediate impact parameter which would be about the same whatever the bombarding energy is. If for this centrality a massive fragment emission from the neck region sets in, the sudden change of the  $Z_{max}$  distribution could be related to a sudden decrease of the QP source mass, i.e. to a geometrical effect. This interpretation is discussed in sections 5.1 and 5.2. .

### 5.1 The role of midrapidity emission.

Dynamical effects were clearly recognized in nucleus-nucleus collisions in the intermediate energy regime. We already noticed in figure 4 the possible role of neck emission which has been extensively studied in reference[24,34,35]. A generalization of the results of reference[34] is shown in figure 13 where the angular distributions of the heaviest fragment ( $Z_{max1}$ ) are drawn for various  $E_{trans}$  bins. The abscissa is the cosine of its emission angle in the QP frame.

For this analysis, the QP centre of mass has been calculated including all products with  $Z \geq 2$  emitted forward in the ellipsoid frame in order to be able to treat events with a residue and no intermediate mass fragment (IMF:  $Z \geq 3$ ). The distributions would be flat for isotropic emission which is not the case. Mostly, the heaviest fragment is forward emitted in the QP frame. This feature is a clear entrance channel memory: full equilibrium has not been achieved at least for most events and light IMF or LCP are emitted at mid-rapidity between the QP and QT. What is the role of this mid-rapidity emission? Does it contribute significantly to the sudden increase of the fragment multiplicity when passing from the residue-like class to the multifragmentation one?

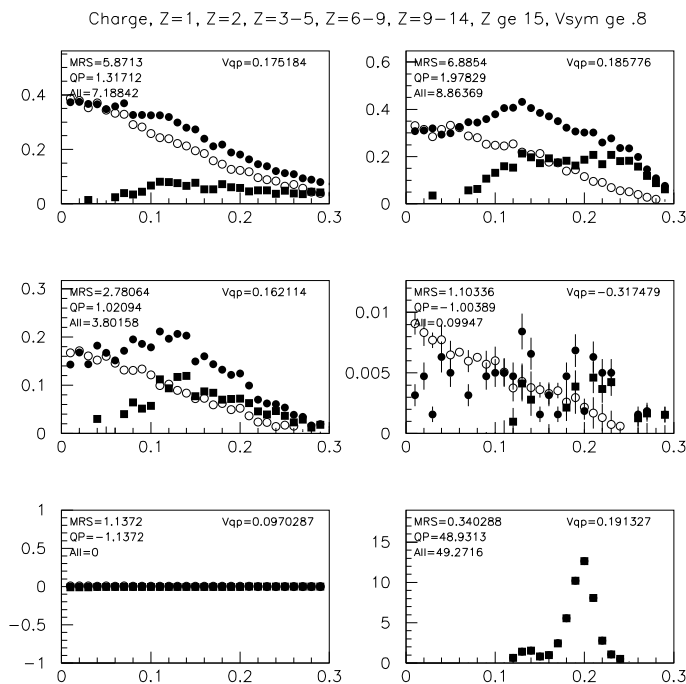


Fig. 14. Charge density distributions for various IMF charges as a function of the parallel velocity to the beam in the c.m. frame in c units. The full and open circles are the distributions for *Etrans* bins 3 and 9 respectively. They have been normalized for zero velocity. The black squares correspond to the difference between the two previous distributions. For the third bin the events with  $Z_{asym}$  larger than 0.8 have been selected. System Au + Au at 100 MeV/u.

In order to evaluate the role of mid-rapidity we performed an analysis based on the hypothesis that mid-rapidity emission comes mainly from the overlap region between the projectile and the target and that its kinematical properties are the same for all the impact parameters. This assumption is in agreement with the basic hypothesis of the HIPSE model[37] which is discussed in section 5.2.

Central collisions are those for which the overlap between the projectile and the target is the largest: the overlap or participant zone is in this case the unique source for particle emission. The corresponding velocity properties have

been assumed to be the reference properties of mid-rapidity emission at any impact parameter (similar parallel velocity distribution shapes for any impact parameter). They have been summarized in plotting the charge density  $\rho$  as a function of the velocity parallel to the beam  $v_{par}$  in the centre of mass frame.

The Au + Au system at 100 MeV/u will be taken as an example. Central collisions have been associated with the largest *Etrans* bin. As a matter of fact, one may see in figure 4 that the  $v_{par} - v_{per}$  plots for the ninth bin is dominated by mid-rapidity emission with a negligible contribution of QP or QT emissions. Now, we focused on the third *Etrans* bin where the bimodality signal is seen. In figures 14 (resp. 15) we have plotted the  $\rho(v_{par})$  distributions for several IMF charges and for  $Z_{asym}$  larger than 0.8 for residue-like selection (resp. lower than 0.2 for multifragmentation). The black dots correspond to the data. The open ones are the corresponding reference distribution obtained for central events (ninth bin). The two distributions have been normalized at zero velocity which means that we assumed that the contribution of the QP at mid-rapidity was negligible. The difference between the two distributions (black squares) is attributed to the sequential QP decay. In figure 14 the statistics is very poor for  $Z$  between 6 and 14 because very few IMF are emitted when a residue is released. On the contrary, a larger number of IMF is obtained when one selects multifragmentation (figure 15). The resulting QP contributions (black squares) for all charges are symmetric around the QP velocity derived from the bottom right frame as it is expected for late sequential decay. This means that any QP decay contribution with an influence from the QT partner, which would show a higher yield of particles in the backward direction[38,39], has been included in the mid-rapidity contribution. The contribution attributed to the QP in this analysis is hence underestimated.

$Z_{asym}$	$Z$	$M_{tot}$	$M_{QP}$	$M_{mi-rap}$	$Z_{tot}$	$Z_{QP}$	$Z_{mi-rap}$
$> 0,8$	LCP	11.62	2.3	9.31	16.1	3.3	12.7
$> 0,8$	IMF	2.14	1.36	0.77	53.2	47.8	5.3
$> 0,8$	Total	13.76	3.66	10.08	69.2	51.1	18.1
$< 0,2$	LCP	14.89	2.37	12.51	21.0	4.2	16.8
$< 0,2$	IMF	5.06	3.00	2.06	47.3	36.9	10.4
$< 0,2$	Total	19.95	5.37	14.57	68.3	41.1	27.2

Table 1

Repatriation between the equilibrated QP and the mid-rapidity of the total available charge forward emitted in the centre of mass. The first three lines are for the residue-like events. The three last ones correspond to multifragmentation events. They all belong to the third *Etrans* bin for which bimodality is observed.  $M_{mi-rap}$ ,  $M_{QP}$ ,  $M_{tot}$  are the multiplicities respectively associated to mid-rapidity, QP emission, and any emission for LCP or IMF or any charged product.  $Z_{mi-rap}$ ,  $Z_{QP}$ ,  $Z_{tot}$  are the corresponding charges. Au + Au system at 100 MeV/u.

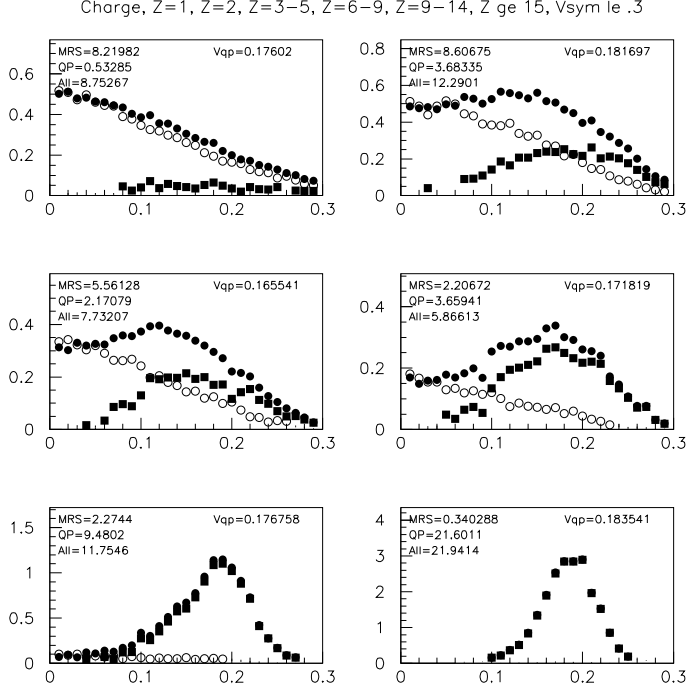


Fig. 15. Similar to figure 14 but the events selected for the third bin are multifragmentation events ( $Z_{asym}$  lower than 0.2).

One may now deduce from the above treatment the minimum QP charge or the maximum mid-rapidity contribution in the third  $Etrans$  bin of interest, i.e. when bimodality is observed. The results are indicated in table 1. The mid-rapidity contribution is never dominant and the mean IMF multiplicity attributed to the QP increases from 1.36 to 3 from residue like to multifragment events. This result seems to indicate that the bimodality signal (disappearance of the residue and strong increase of IMF production) is not dominated by mid-rapidity emission.

## 5.2 Comparison with a dynamical model.

The role of dynamics has been tested with the help of the event generator HIPSE[37] in which the geometry of the collision is explicitly taken into account. For any impact parameter the overlap region leads to mid-rapidity emission, and contributes to QP excitation from nucleon-nucleon collisions. This is thus particularly suited to explore the puzzling property observed in figures 11 and 12: the bimodality transition is always observed for similar impact parameters corresponding to a  $Etrans$  value which increases roughly proportionally with the beam energy. The parameters of the model have been adjusted in order to reproduce most of the experimental inclusive distributions (charge, angular and energy distributions) for Xe+Sn reactions between 25 and 50 MeV/u. The global experimental features are well reproduced by

the model, as shown in figure 16 for the Xe + Sn system at 80 MeV/u. This figure is similar to the experimental one (figure 8) and one recognizes bimodal distributions in the third and the fourth bins in very good agreement with the data. In the model, it is possible to go further and search the reason why the residue production vanishes when  $E_{trans}$  is increased. The reason for this change is not directly the fact that a decrease of the impact parameter leads to a smaller QP spectator. This conclusion may be drawn from figure 17 in which is shown the correlation between the initial hot QP size and  $Z_{asym}$  for the nine  $E_{trans}$  bins. It turns out that the initial QP size is always large. This is especially the case for bins 3 and 4, i.e. in the region where bimodality is observed in figure 16. This result means that it is the decay step which is responsible for the disappearance of the residue. It is found from the model that both the excitation energy and the angular momentum of the QP become quite large (3-5 MeV/u and  $70\hbar$ ) when the abrupt change in the decay mechanism is observed. In reference [40], by using a sequential decay code, the authors conclude that the angular momentum is the key parameter. To progress on the understanding of the nature of the transition it will be necessary to perform similar simulations with a non-sequential decay code and, from the experimental point of view, to compare systems with very different values of angular momentum but similar excitation energies in the range of 3-5 MeV/u.

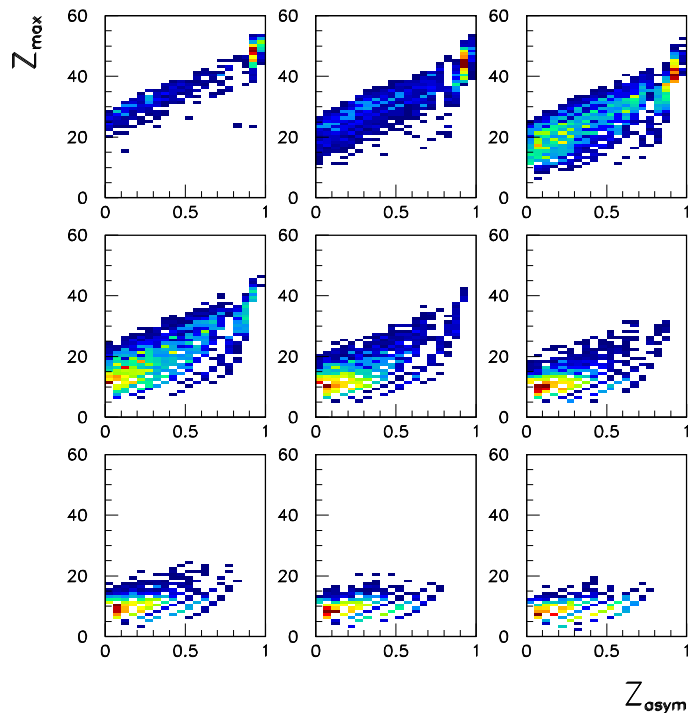


Fig. 16.  $Z_{asym} - Z_{max}$  plots for the 9  $E_{trans}$  bins as it is calculated by the HIPSE event generator. Xe+Sn system at 80 MeV/u.

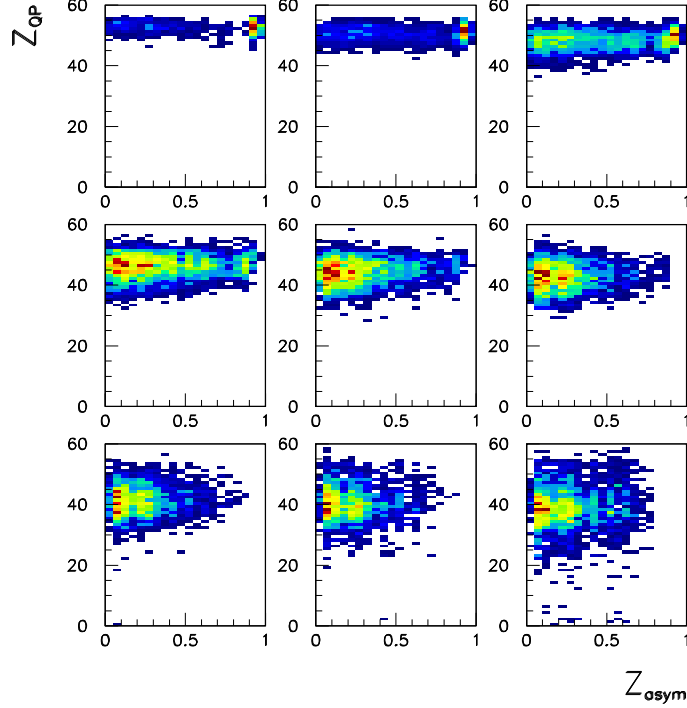


Fig. 17.  $Z_{asym} - Z_{QP}$  plots for the 9 *Etrans* bins as it is calculated by the HIPSE event generator. Xe+Sn system at 80 MeV/u.

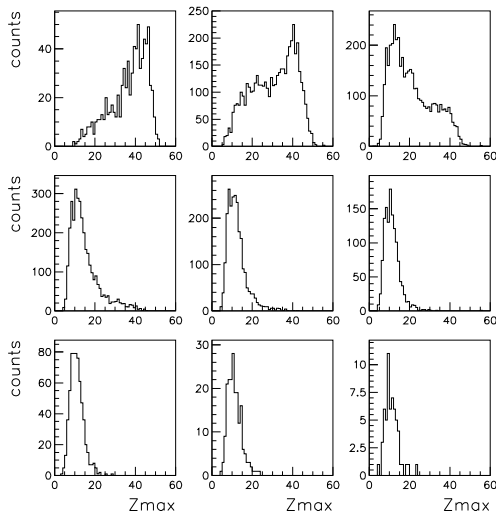


Fig. 18.  $Z_{max}$  distributions for the 9 *Etrans* bins when the "less dynamical events" (see text) are selected. Xe+Sn system at 80 MeV/u.

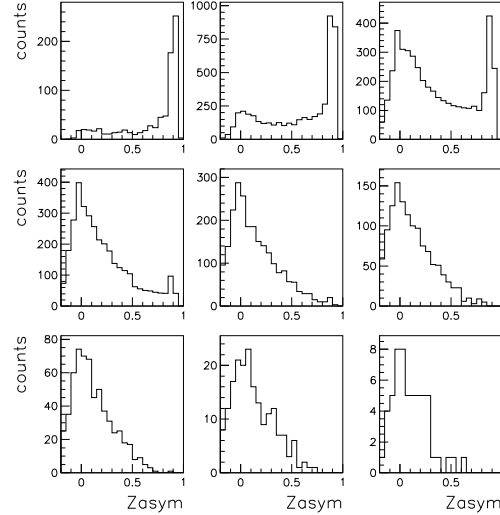


Fig. 19.  $Z_{asym}$  distributions for the 9 *Etrans* bins when the "less dynamical events" (see text) are selected. Xe+Sn system at 80 MeV/u.

### 5.3 Test of preequilibrium effects

As shown in section 5.1, the angular distributions of the heaviest fragment, ( $Z_{max1}$ ), are forward peaked (figure 13), which indicates a memory of the en-



trance channel. Nevertheless, for some events, the heaviest fragment is emitted backward in the QP frame. The memory of the entrance channel is weaker for these events which will thus be labelled "less dynamical events". In figures 18 and 19, they have been isolated in selecting  $\cos(\theta)$  values lower than  $-0.4$  (see figure 13). By comparison with those obtained when this condition is not required (figures 9 and 10), two facts may be emphasized: firstly the bimodal behaviour is better evidenced when the "less dynamical events" are selected. This is especially the case for the  $Z_{asym}$  variable which exhibits clearly a double humped distribution in the third  $Etrans$  bin. On the other hand, the transition takes place for a lower  $Etrans$  value for these selected events. All these features are expected if bimodality reflects a thermal behaviour. Indeed, lattice-gas calculations (figure 2) indicate that the bimodality signal is attenuated by dynamical effects; the observed difference between the two samples of events may be explained in this framework. Moreover, when dynamical effects are present, we can expect the value of  $Etrans$  at the transition point to be increased since the contribution of a non-relaxed energy component does not modify significantly the bimodality signal.

## 6 Transition excitation energies and temperature

To progress in the understanding of the bimodality signal, in this section, we try to connect its properties to signals of liquid-gas transition. If fragmentation can be associated to such a transition, then a bimodality should be observed in the probability distribution of the system density which is the order parameter of the transition. Two measurable variables strongly correlated to the density are the size of the heaviest fragment and the energy: both should have bimodal probability distributions in the liquid-gas transition as illustrated in the framework of the lattice-gas model in figure 20. On the experimental side, the matter density is not accessible but the excitation energy can be obtained from calorimetry as described in section 6.1.

### 6.1 QP reconstruction

In order to be able to characterize the QP, one has to identify its centre of mass and its excitation energy. As discussed in section 2.1, any product emitted forward in the ellipsoid frame has been attributed to the QP. In order to minimize the contribution of midrapidity, we have calculated the origin of the QP frame from the IMF only ( $Z \geq 3$ ) at variance from section 5.1. Then, we have estimated the deposited energy from calorimetry in including all the IMF and only the LCP forward emitted in the QP frame. The LCP contribution has been doubled to account for backward emitted LCP. This

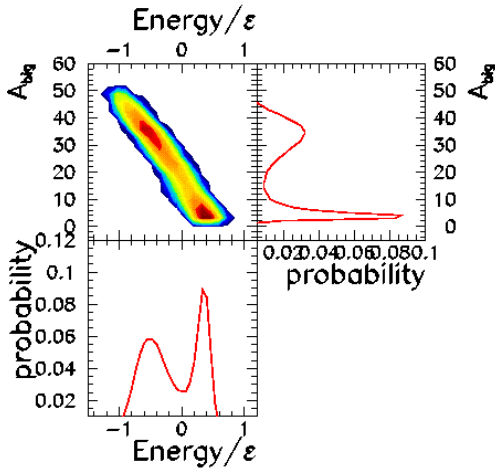


Fig. 20. Correlation between the largest fragment size and the internal excitation energy from lattice-gas calculations close to the transition temperature (see ref [13]). The projections are also shown. Bimodality is observed for both variables.

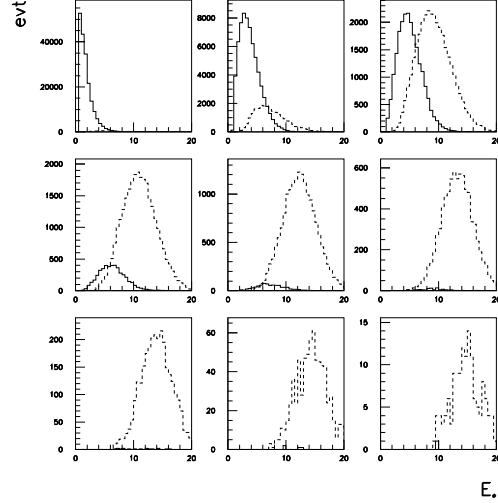


Fig. 21. Excitation energy (MeV/u) distributions for various  $E_{trans}$  bins. The events have been separated in two classes corresponding to the 2 bimodality solutions:  $Z_{asym} \geq 0.7$  (full line histograms) and  $Z_{asym} \leq 0.3$  (dashed line histograms). Xe+Sn system at 80 MeV/u.

procedure permits to avoid to a large extent LCPs resulting from mid-rapidity emission. The charge of the original QP has been determined by adding the detected product charges. Its mass has been taken as that giving the same N/Z ratio as the projectile. The masses of the fragments (for Z exceeding 4) have been given by the EPAX formula[42] and the neutron number has then been obtained from the difference between the initial QP mass and the total masses attributed to the detected products. Then the excitation energy has been calculated from:

$$E^* = \sum_{i=1}^{M_{IMF}} T_i + \sum_{j=1}^{M_{LCP}} T_j + M_{neut} \langle T_n \rangle - Q \quad (2)$$

where the  $T_{i,j,k}$  values are the kinetic energies for each product,  $M_{IMF}$ ,  $M_{LCP}$  and  $M_{neut}$  are the multiplicities of IMF, LCP and neutrons and  $Q$  the mass balance. The average kinetic energy of neutrons  $\langle T_n \rangle$  has been obtained by means of an effective temperature[45,46].

## 6.2 Excitation energy distributions

In figure 21, the excitation energy distributions are shown for various  $E_{trans}$  bins and for the Xe + Sn system at 80 MeV/u. For each  $E_{trans}$  bin, we

have separated the events corresponding to  $Z_{asym}$  larger (resp. lower) than 0.7 (resp. 0.3). The two distributions have similar amplitudes in the third bin in which the bimodality signal is observed (see figure 8) but they do not coincide. Even if excitation energies as high as 15 MeV/u are certainly not realistic, we can see that a larger mean excitation energy is measured for the multifragmentation case (low  $Z_{asym}$ ) in qualitative agreement with the calculation results of figure 20. Many reasons can be invoked to explain the fact that these two distributions overlap more strongly than the model calculation results: the sorting is not a canonical one; moreover, the calorimetry method is far from being perfect due to the doubling procedure and to the estimated neutron correction[47].

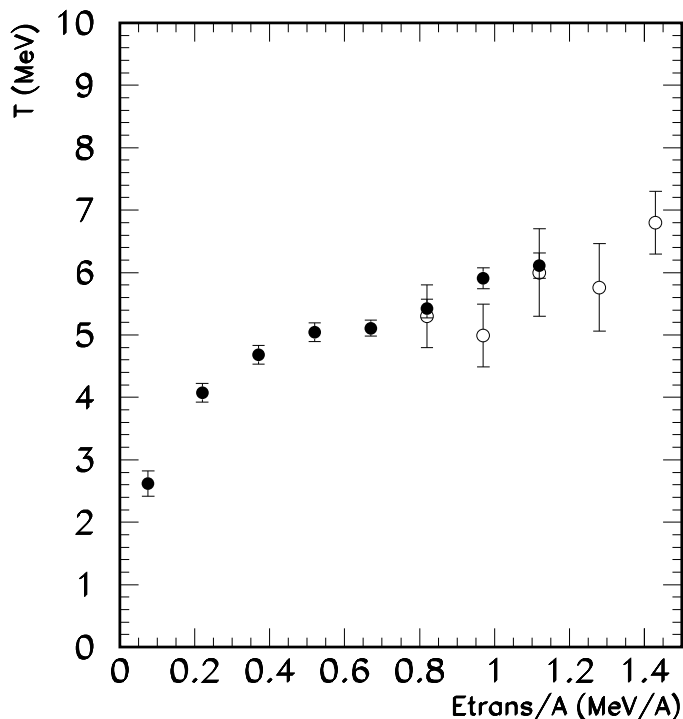


Fig. 22. Temperatures measured as a function of  $E_{trans}$  for residue and multifragment events. Xe+Sn system at 80 MeV/u. The black (resp. open) points correspond to two thermometers: slope parameter of protons (resp. double isotopic ratio method). The error bars are statistical. The transition region is around  $E_{trans}/A = 1 \text{ MeV}/u$  (figure 11).

### 6.3 Temperatures

One may now try to measure the involved temperatures. If bimodality has a thermal origin, one would expect to observe similar temperatures for both classes of events: residue-like events and multifragmentation.

Temperature measurement is a difficult task because the various possible ther-

thermometers are not equally suited to the different energy regimes. The kinetic energy slope method is expected to be adapted when a residue is released, but not in the multifragmentation case because the particle source is not unique. The double isotopic ratio is better suited in this second case because the system can explore a small density region[48] and because the IMF multiplicity is significant. In figure 22, we indicate the corresponding results for the four first bins of figure 21. The abscissa is the transverse energy normalized to the system size and the ordinate indicates the measured temperatures. The double isotopic ratio method (He-Li nuclei) has been used for the events selected with  $Z_{asym}$  lower than 0.3 and the corresponding results have been corrected for side feeding effects[48]; the slope of proton spectra (forward emitted in the QP frame) has been used for the residue events ( $Z_{asym}$  larger than 0.7). The points with low statistics have not been plotted. In the transition energy region (0.8 – 1.2 MeV/u), both groups exhibit similar temperature values as expected if bimodality has a thermal origin.

The events belonging to the two regions of the bimodal distribution are thus found to correspond to different excitation energies but to similar temperatures. It is what is expected for a first order phase transition for which the energy jump between the two solutions reflects the latent heat. This result is hence coherent with a thermal origin of multifragmentation but cannot be considered as a strong evidence because the compared temperatures have been obtained with two different thermometers.

## 7 Bimodality and other possible phase transition signals

As mentioned in the introduction, several signatures of phase transition have been proposed and experimentally observed. Due to the various experimental conditions, each of these signals present some weaknesses. Thus the occurrence of a phase transition would be strongly reinforced by a simultaneous observation of several signatures. Such is the aim of this section.

### 7.1 Relation between bimodality and $\Delta$ -scaling

$\Delta$ -scaling is a signal proposed in the framework of the universal fluctuation theory [14]. It may be used to distinguish between different phases and to identify critical points.  $\Delta$ -scaling is observed for an order parameter  $m$  if the probability  $P_N(m)$  for observing a given value of  $m$  can be written with the following formula

$$\langle m \rangle^{\Delta} P_N(m) = f(z_{\Delta}) = f\left(\frac{m - \langle m \rangle}{\langle m \rangle^{\Delta}}\right) \quad (3)$$

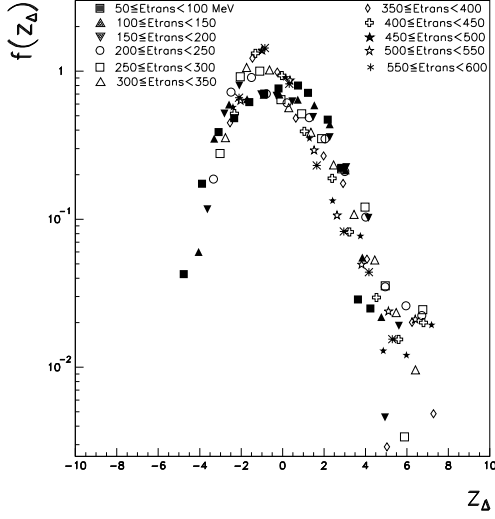


Fig. 23. Normalized  $Z_{max}$  distributions according to equation 3 for the system Xe+Sn at 80 MeV/u with  $\Delta=0.5$ . Various symbols correspond to various  $E_{trans}$  bins.

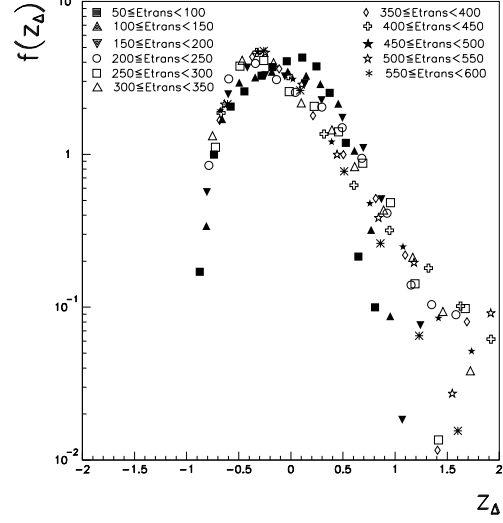


Fig. 24. Similar to figure 23 with  $\Delta=1$ .

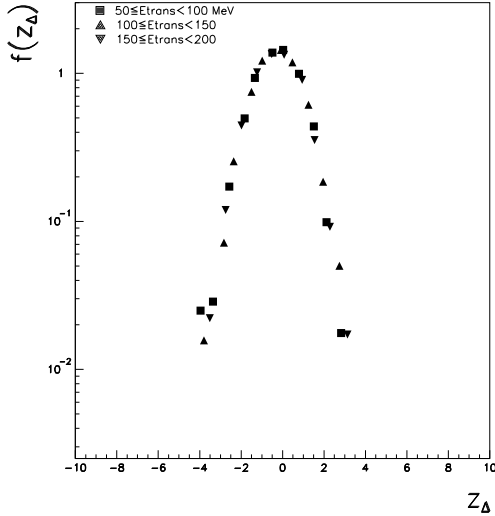


Fig. 25. Delta scaling for the system Xe+Sn at 80 MeV/u with  $\Delta=0.5$ . Only residue like events ( $Z_{asym}$  larger than 0.7) have been retained. Various symbols correspond to various  $E_{trans}$  bins. Only the  $E_{trans}$  bins for which the residue contribution is dominant have been retained.

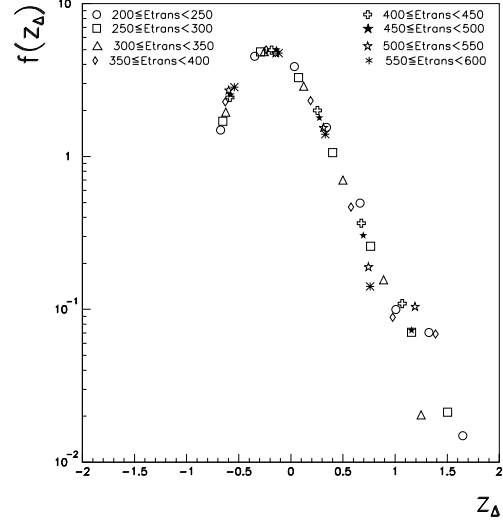


Fig. 26. Delta scaling for the system Xe+Sn at 80 MeV/u with  $\Delta=1$ . Only multifragmentation events ( $Z_{asym}$  lower than 0.3) have been retained. Various symbols correspond to various  $E_{trans}$  bins. Only the  $E_{trans}$  bins for which the multifragmentation contribution is dominant have been retained.

in which  $f(z_\Delta)$  is a universal function which does not depend on the size  $N$  of the system. For a system exhibiting two phases, the  $\Delta$  value is expected

to be close to 0.5 for an ordered phase and to 1 for a disordered phase. The transition point between the two phases is first order if, at this point, the distribution of  $m$  is bimodal, and second order if it obeys  $\Delta=1$  scaling with a non-Gaussian tail[14]. Several data have been analyzed in this context[6,7]. In reference [7]  $\Delta$ -scaling was evidenced for central collisions for the Xe + Sn and Au + Au systems of interest in the present paper. Those results indicate that the size of the largest fragment is an order parameter. The ordered (resp. disordered) behaviour is observed below (resp. above) an incident energy of 39 MeV/u for the Xe+Sn system. In these works, the nature of the transition could not be determined.

We tested such a behaviour for the semi-peripheral collisions of interest in the present paper. In figures 23 and 24 the  $f(z_\Delta)$  functions (with  $m = Z_{max}$ ) are plotted for various *Etrans* bins for the 80 MeV/u Xe + Sn system. The plots correspond to  $\Delta$  values of 0.5 and 1 respectively. No scaling is observed. However, scaling is recovered if one separates the events according to the  $Z_{asym}$  ranges corresponding to defined events: residues ( $Z_{asym}$  larger than 0.7) or multifragmentation ( $Z_{asym}$  smaller than 0.3). The results are shown in figures 25 and 26. Residue events are numerous only for *Etrans* values smaller than 200 MeV. Only the corresponding bins have been retained in figure 25. Conversely, multifragmentation becomes dominant for *Etrans* larger than 200 MeV. Only the corresponding bins have been retained in figure 26. Similar results have been obtained for the Au+Au system with fission events reconstructed as explained in section 3[49].

The fact that the scaling is clearly observed for the two classes of events suggests that these latter can be understood as an ordered (resp. disordered) phase. Conversely, the absence of scaling for the global distribution is consistent with the interpretation in terms of phase coexistence. Indeed, the absence of bimodality in the distribution of  $Z_{max}$  may be due to a too strong correlation between the sorting variable and the deposited energy, which is also an order parameter: if a constraint is applied on an order parameter in the coexistence zone, its bimodal character is naturally suppressed. As the system is still in the coexistence zone, a pure phase scaling may be expected to fail as it is suggested in recent theoretical calculations[15].

## 7.2 Relation between bimodality and negative heat capacity

Another signal of phase transition is negative heat capacity. This phenomenon is univocally associated to first order phase transitions with a finite latent heat in isolated systems with a size comparable to the range of the forces governing its equation of state[36]. A negative heat capacity occurs whenever the entropy presents an anomalous curvature as a function of the available energy. It has

been shown in reference [17] that heat capacity may be deduced from the measurement of the fluctuations in the sharing of the available energy between independent degrees of freedom. Since the heat capacity can be negative only in the microcanonical ensemble, from an experimental point of view events with a defined excitation energy have to be selected. For such a sorting, the total heat capacity may be approximately written:

$$C \approx \frac{C_1^2}{C_1 - \frac{\sigma^2}{T^2}} \quad (4)$$

where  $C_1$  is the partial heat capacity for a subset of degrees of freedom (for instance momentum space),  $T$  is the temperature and  $\sigma^2$  is the variance associated with the sharing of the total available energy between the degrees of freedom subset and the other ones. The total heat capacity becomes negative when these fluctuations become larger than the fluctuations associated to the canonical ensemble.

This formalism has been used to study central Xe + Sn collisions from 32 to 50 MeV/u [2], and peripheral Au + Au collisions at 35 MeV/u [1]. In both cases, fluctuations exceeding the canonical expectation were found. For the Xe + Sn central collisions, the signal is observed at 32 and 39 MeV/u but not at larger bombarding energies for which the system would have left the coexistence region.

We have tried to correlate this signal with the bimodality one which is discussed in this paper. For this purpose, events must be sorted according to the excitation energy of the QP, obtained by calorimetry on the QP source as explained in section 6.1. We have retained only events with a total reconstructed source charge equal to the projectile charge within 10%.

The negative heat capacity study has been performed in studying the sharing of the excitation energy between the kinetic and the potential energy parts at the freeze-out configuration. Rewriting equation 4 in normalizing the heat capacity to the source size gives:

$$C \approx \frac{C_k^2}{C_k - \frac{\langle A_{sou} \rangle \sigma_k^2}{T^2}} \quad (5)$$

$\sigma_k^2$  is the variance of the kinetic energy distribution;  $\langle A_{sou} \rangle$  is the average mass number of the source;  $C_k$  is the partial kinetic energy heat capacity per nucleon:

$$C_k = \frac{d \langle \frac{E_k}{A_{sou}} \rangle}{dT} \quad (6)$$

The potential energy  $E_p$  has been obtained from the mass balance corrected for the Coulomb part in assuming that all the LCP are emitted from the IMF in a second step after the freeze-out:

$$E_p = \left( \sum_{i=1}^{M_{IMF}} m_i - m_{sou} \right) + E_{coul} \quad (7)$$

$M_{IMF}$  is the IMF multiplicity ( $Z \geq 3$ ); the  $m_i$  are the IMF primary masses;  $m_{sou}$  is the reconstructed QP mass; the Coulomb energy balance at freeze-out  $E_{coul}$  has been calculated from the Wigner-Seitz formula[50].

The temperature of relation 5 has been calculated from the total kinetic energy by using for the level density parameter  $a_i = \frac{A_i}{8}$ :

$$\langle E_k \rangle = \left\langle \sum_{i=1}^{M_{IMF}} a_i \right\rangle T^2 + \left\langle \frac{3}{2}(M-1) \right\rangle T \quad (8)$$

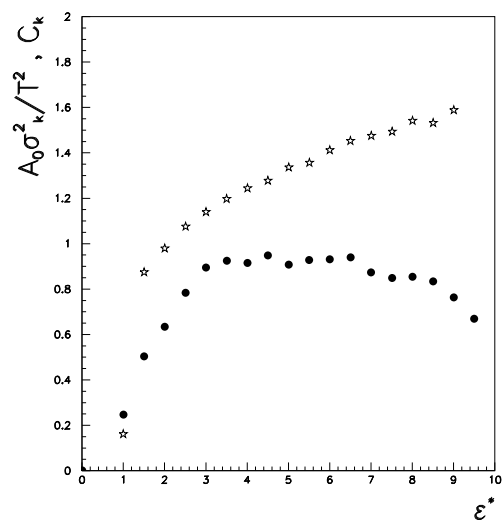


Fig. 27. Evolution with the available excitation energy in  $MeV/u$  of the two terms of the denominator of relation 5 (see text): partial heat capacity (open stars), and fluctuation term (black points). System Au + Au at 80 MeV/u.

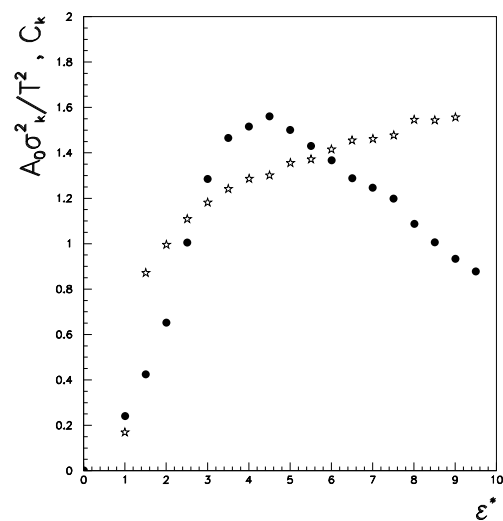


Fig. 28. Similar to figure 27 but in selecting the most compact QP events: see text.

From equation 5 it turns out that the heat capacity will be negative if the second term of the denominator (fluctuation term) exceeds the first one (partial heat capacity). These two terms are plotted in figure 27. Fluctuations are far below the canonical expectation whatever the excitation energy is. This result is quite general and has been observed for quasi-projectiles from the Xe + Sn and Au + Au systems at any bombarding energy.



At this point, one may recall that the negative heat capacity signal is much more fragile than the bimodality one. First, the evaluation of fluctuations is very sensitive to the details of the calorimetric hypotheses and side feeding corrections[51]. Moreover, any energy fraction which has not been shared among all the available degrees of freedom but is still stored in some selected ones will induce a decrease of the fluctuations we are looking at. In other words, negative heat capacity is not observed if dynamical effects freeze a sizeable part of the available energy in a few defined degrees of freedom reminiscent of the initial direction of the beam. In order to decrease the influence of dynamical effects, we have tried to select QP events in which the memory of the entrance channel is minimized. We did such a selection in section 5.3 in cutting the  $\cos(\theta)$  distribution of figure 13). This cut does not modify significantly the signal. To ensure a stronger reduction of dynamical effects, we selected compact events, i.e. events for which the QP decay is not elongated in the momentum space. Compactness has been estimated from the relative velocity between the largest QP fragment and the mean velocity of the other QP fragments:

$$v_{rel} = v_{Z_{max}} - \frac{\sum_{i=1}^{M_{IMF}-1} A_i v_i}{\sum_{i=1}^{M_{IMF}-1} A_i} \quad (9)$$

A larger value  $v_{rel}$  is expected if intermediate velocity IMF contribute to the QP. We have retained only the events for which  $v_{rel}$  was smaller than 3 cm/ns which is a value expected from Coulomb repulsion. The corresponding results are shown in figure 28. Only with this selection, abnormal fluctuations appear for excitation energies between 3 and 5–6 MeV/u. This is a general feature for the Au + Au system as shown in figure 29 while, at variance, the fluctuations remain below their canonical expectation for any excitation energy for the Xe + Sn system (see figure 30). This difference between the two systems is not fully understood.

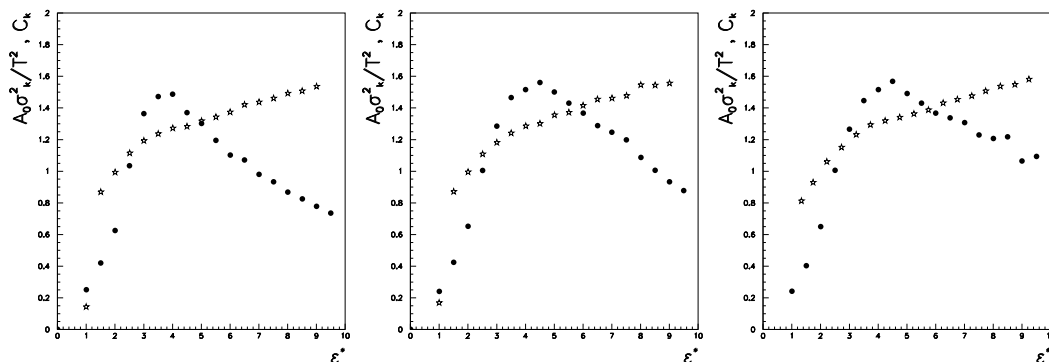


Fig. 29. Systems Au + Au at 60 (left), 80 (middle) and 100 (right) MeV/u. Evolution with the available excitation energy of the two terms of the denominator of relation 5: partial heat capacity (open stars), and fluctuation term (black points). Non compact events (see text) have been rejected.

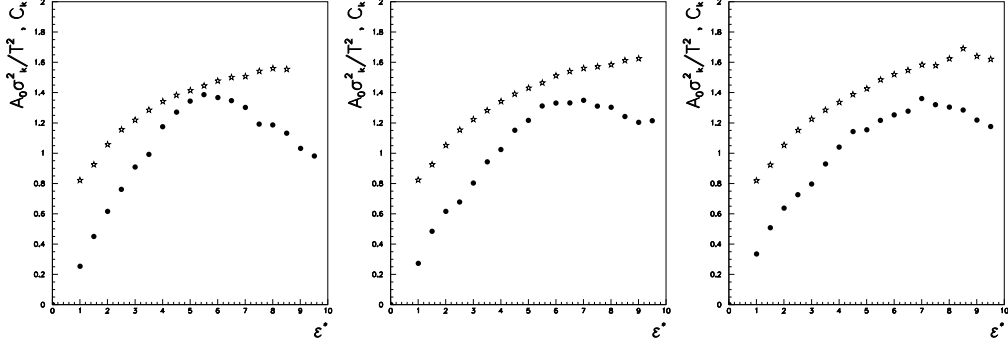


Fig. 30. Systems Xe + Sn at 65 (left), 80 (middle) and 100 (right) MeV/u. Evolution with the available excitation energy of the two terms of the denominator of relation 5: partial heat capacity (open stars), and fluctuation term (black points). Non compact events (see text) have been rejected.

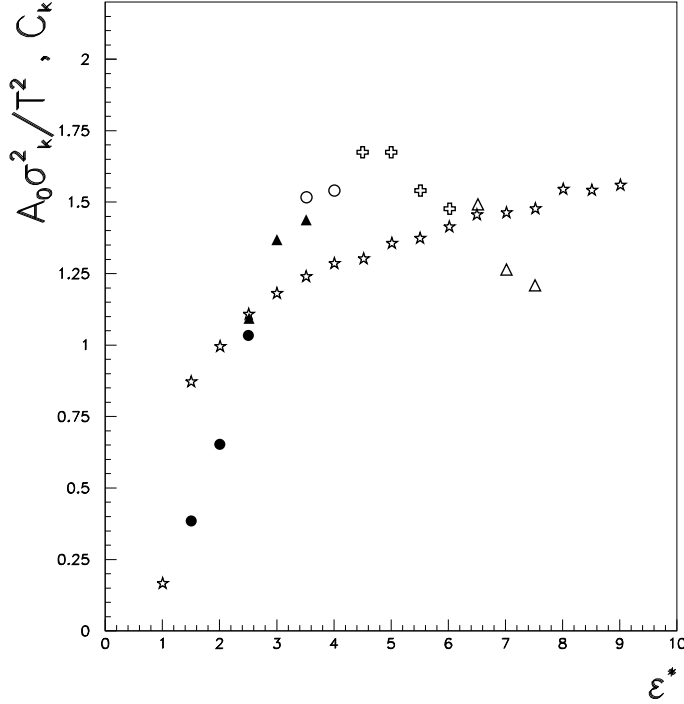


Fig. 31. Similar to figure 28 for the Au + Au 80 MeV/u system but the events have been sorted according to  $E_{trans}$ . Each symbol corresponds to a selected  $E_{trans}$  bin of 0.25 MeV/u width. The fluctuation peak is observed in the bins associated with the open points and to the crosses covering an  $E_{trans}/u$  range from 0.65 to 1.15 MeV/u) in which the bimodality transition has been observed in figure 11.

Let us focus now on the Au + Au system for which fluctuations are more important. One may first remark that the excitation energy range corresponding to the fluctuation peak is quite independent of the bombarding energy. In figure 31 we have connected this signal with the bimodality one. Events have been sorted according to the  $E_{trans}$  variable used previously for bimodality studies and only the most probable excitation energy bins have been retained

for each  $E_{trans}$ . Each symbol of figure 31 corresponds to an  $E_{trans}$  bin. The fluctuation peak corresponds to the third (open points) and fourth (crosses) bins, i.e. for  $E_{trans}/u$  values covering the range [0.65-1.15 MeV/u] in which the bimodality transition has been observed in figure 11. This coherence indicates that abnormal fluctuations and bimodality may sign the same physical phenomenon for the same set of events, but sorted in two different ways.

## 8 Conclusion

We studied two symmetrical systems Xe + Sn and Au + Au from 60 to 100 MeV/u. We focused on semiperipheral collisions for which it is possible to isolate a QP contribution. The sorting of the collisions has been achieved from the LCP transverse energy on the QT side and we observed QP properties thus avoiding as much as possible auto-correlation due to sorting. We selected events for which most of the available charge on the QP side has been detected and identified. The distribution of the charge of the heaviest fragment and the asymmetry between the two heaviest fragments produced in each event was analysed. We have observed a two-peaked distribution for all systems for a temperature range around 5 MeV. One peak corresponds to events dominated by a residue and the other one to multifragmentation. Fission events in the Au case have been treated together with the residue-like events. If this behaviour is strongly suggestive of a phase transition, it does not allow to conclude about the nature of the phenomenon.

We observed a scaling on the total mass of the system since the transverse energy for which bimodality is observed is proportional to this mass for a defined bombarding energy per nucleon. On the other hand, we observed a transition transverse energy roughly proportional to the beam energy. We interpreted this effect as due to pre-equilibrium effects which increase with the bombarding energy. This statement is supported by the fact that the bimodality signal is observed for smaller transverse energy values if one selects events which are closer to equilibrium. This interpretation is still open to discussion. Nevertheless, it turns out that many features are in agreement with an interpretation in terms of a phase transition in which the major parameter is the deposited energy. As a matter of fact, it has been established that the deposited (excitation) energies at the transition are larger for multifragmentation than for the residue-like events. At the same time, it has been shown that the temperatures involved in both cases are similar. This second conclusion is however weakened by the fact that the available thermometers are different for the two sets of events.

A very interesting feature is that the bimodality signal can be correlated with defined scaling properties in the distribution of the heaviest fragment size

and the observation of important configurational energy fluctuations which we have tentatively associated at least for the Au+Au system to negative heat capacity.

Altogether this set of results is in agreement with the expectations from a phase transition belonging to the liquid-gas universality class, and is well reproduced by a dynamical model. Many points need to be clarified. If the convexity can be seen in the  $Z_{max}$ - $Z_{asym}$  representation, this convexity is not very pronounced and cannot be observed in the  $Z_{max}$  distribution. This leaves the question of the order of the transition open. The relevant order parameter and the associated nature of the transition is not clear either. In particular the dynamical code HIPSE suggests that angular momentum may play a major role in the transition.

Up to now, bimodality has been mainly recognized in semiperipheral collisions. The fact that it is more difficult to observe it in central ones may reflect a lower involved angular momentum. But it can also be due to the fact that the central collision sorting is too close to a microcanonical selection (for which bimodality should not be observed) rather than a canonical one ensuring the energy fluctuations which are necessary to observe the coexisting phases. In order to better elucidate this question, we intend to progress in two directions. We will first concentrate on a better understanding of central collisions in mixing various bombarding energies to simulate a canonical sorting. Another kind of analysis will concern the understanding of the role of the distance to equilibrium which is reached for a set of events. We will address this question in comparing collisions with an entrance channel which is asymmetric in isospin. The distance to equilibrium will be inferred from the distance to equilibrium in the isospin degree of freedom. Such measurements have been performed with INDRA at GSI for the  $^{129}\text{Xe} + ^{112}\text{Sn}$  et  $^{124}\text{Xe} + ^{124}\text{Sn}$  at 100 MeV/u.

## References

- [1] M. d'Agostino et al., Nucl. Phys. A650 (1999) 329.
- [2] N. Le Neindre et al., Proceed. of the XXXVIII Int. Wint. Meet. on Nuc. Phys., Bormio, 2000, p. 404, and N. Le Neindre, PhD thesis, Caen (1999), <http://tel.ccsd.fr/documents/archives0/00/00/37/41>.
- [3] G. Tabacaru et al, Eur. Phys. J. A 18 (2003) 103.
- [4] B. Tamain et al (INDRA and ALADIN collab.) Proceedings of the IWM meeting, Caen, p. 83 (2003).
- [5] M. Pichon et al (INDRA and ALADIN collab.), Proc. of the XL1st Winter Meeting on Nucl. Phys., Bormio, Italy, Jan. 26 - Feb. 1, 2003, Ricerca Scientifica ed Educatione Permanente, Suppl. 120 (2003), ed. by I. Iori and A. Moroni, p. 149.
- [6] R. Botet et al, Phys. Rev. Lett. 86 (2001) 3514.
- [7] J. Frankland et al. (INDRA-ALADIN collaborations), Phys. Rev. C71 (2005) 34607.
- [8] J.B. Elliott et al., Phys. Rev. Lett. 88 (2002) 042701.
- [9] B. Borderie et al (INDRA collab.), Eur.Phys. J. A6 (1999) 197.
- [10] J. Pochodzalla et al (ALADIN collab.), Phys. Rev. Lett. 75 (1995) 1040.
- [11] J. Natowitz et al., Phys. Rev. C65 (2002) 034618.
- [12] K. Binder and D.P. Landau, Phys. Rev. B30, 1477 (1984).
- [13] Ph. Chomaz and F. Gulminelli, "Dynamics and thermodynamics with long range interactions", Lectures Notes in Physics Vol. 602, Springer (2002); P. Chomaz, F. Gulminelli, V. Duflot, Phys. Rev. E64 (2001) 046114.
- [14] R. Botet and M. Ploszajczak, Phys. Rev. E62 (2000) 1825.
- [15] F. Gulminelli and P. Chomaz, Phys. Rev. C71 (2005) 054607.
- [16] F. Gulminelli and Ph. Chomaz, Nucl.Phys. A734 (2004) 581.
- [17] Ph. Chomaz and F. Gulminelli, Nucl. Phys. A647 (1999) 153.
- [18] N. Bellaize et al. (INDRA collaboration), Nucl. Phys. A 709 (2002) 367.
- [19] P. Laitesse et al., (INDRA collaboration), Phys. Rev. C71 (2005) 034602.
- [20] B. Borderie, J. Phys. G: Nucl. Part. Phys. 28 (2002) R217.
- [21] J. Pouthas et al, Nucl. Inst. Meth. A357 (1995) 418.
- [22] J. Pouthas et al, Nucl. Inst. Meth. A369 (1996) 222.

- [23] A. Le Fvre et al., Nucl. Phys. A735 (2004) 219.
- [24] J. Lukasik et al., Phys. Rev. C66 (2002) 064606.
- [25] A. Trzcinski et al., Nucl. Instr. and Meth. A501 (2003) 367.
- [26] K. Turzo et al., Eur. Phys. J. A21 (2004) 293.
- [27] C. Escano-Rodriguez and the Indra/Aladin collaborations, preprint nucl-ex/0503007.
- [28] J.F. Dempsey et al, Phys. Rev. C54 (1996) 1710.
- [29] T. Lefort et al., Nucl. Phys. A662 (2000) 397.
- [30] A. Pagano et al., Nucl. Phys. A734 (2004) 504.
- [31] P. Kreutz et al., Nucl. Phys. A556 (1993) 672.
- [32] Y.G. Ma et al., Nucl. Phys. A749 (2005) 106.
- [33] A. Schüttauf et al., Nucl. Phys. A607 (1996) 457.
- [34] J. Colin et al. (INDRA collaboration), Phys. Rev. C67 (2003) 064603.
- [35] E. plagnol et al. (INDRA collaboration), Phys. Rev. C61 (2000) 014606.
- [36] D.H.E. Gross, "Microcanonical thermodynamics: phase transitions in finite systems", Lectures Notes in Physics Vol. 66, World Scientific (2001).
- [37] D. Lacroix, A. Van Lauwe and D. Durand, Phys. Rev. C69 (2004) 054604.
- [38] S.Hudan et al., Phys. Rev. C70 (2004) 031601.
- [39] M. Jandel et al., J. Phys. G: Nucl. Part. Phys. 31 (2005) 29.
- [40] O. Lopez, D. Lacroix and E. Vient, Phys. Rev. Lett. 95 (2005) 242701.
- [41] M.F. Rivet et al (INDRA and ALADIN collaborations), Nucl. Phys. A749 (2005) 73.
- [42] K. Summerer and B. Blank, Phys. Rev. C61 (2000) 034607.
- [43] F. Gulminelli and Ph. Chomaz, Phys. Rev. Lett. 82 (1999) 1402.
- [44] R.J. Charity et al, Nucl. Phys. A483 (1988) 371.
- [45] J.A. Hauger et al., EOS collaboration, Phys. Rev. C57 (1998) 764 and reference quote therein.
- [46] M. d'Agostino, et al, Nucl. Phys. A699 (2002)795.
- [47] E. Vient et al. (INDRA collaboration), Nucl. Phys. A700 (2002) 555.
- [48] H. Xi et al., Phys. Lett. B431 (1998) 8.
- [49] M. Pichon, PhD thesis, Caen (2004), <http://tel.ccsd.cnrs.fr/documents/archives0/00/00/74/51/>.
- [50] J.P. Bondorf et al, Phys. Rep. 257 (1995) 133.
- [51] M.D'Agostino et al., Nucl.Phys. A 699 (2002) 795.